Structural explanation of the rheology of a colloidal suspension under high dc electric fields

Manuel J. Espín, Ángel V. Delgado,* and Fernando González-Caballero
Group of Physics of Interfaces and Colloidal Systems, Department of Applied Physics, Faculty of Science, University of Granada, 18071-Granada, Spain
(Received 16 September 2005; published 7 April 2006)

In this work we describe the electrorheology of suspensions consisting of hematite (α-Fe_2O_3) particles dispersed in silicone oil in the presence of large dc electric fields. If an electric field pulse is applied to the systems, it is possible to estimate the time that the electrorheological (ER) fluid takes to reach its final microstructure in the presence of the field. Our results indicate that response times of several seconds are typical, and that this time decreases with the field strength. Conventional shear-rate sweeps indicate the existence of a well-defined dynamic yield stress and a shear-thinning behavior. Interestingly, both the yield stress and the shear-thinning slope a [relating the viscosity, η, and the shear rate, $\dot{\gamma}$, as $\eta = a\dot{\gamma}^{-b} + \eta(\infty)$] show a linear dependence on the field strength, E, in disagreement with the E^2 dependence often reported. This deviation is associated with changes in the conductivity of the dispersion medium with the field strength. A simple calculation of the interactions present in our ER fluid demonstrates that the ER behavior is entirely controlled by hydrodynamic ($\propto\dot{\gamma}$) and electrical forces ($\propto E$). This is confirmed by the collapse of all experimental results in a single master curve when the relative viscosity is plotted against the ratio $\dot{\gamma}/E$. Careful attention has been paid in this work to the microstructure of the suspensions in the presence of both shear and electric fields simultaneously: the particles gather themselves on the walls of the electrorheological measurement cell, forming aggregates with cylindrical symmetry, shaped as rings or lamellas of solids. The electric field induced increase in viscosity is the consequence of the balance between two actions: that of the electric field, tending to keep particles together, and that of the shear field, forcing the flow of the liquid phase in the regions between rings or between rings and walls.

DOI: 10.1103/PhysRevE.73.041503 PACS number(s): 83.80.Gv

I. INTRODUCTION

The abrupt alteration of the rheological properties of a nonconducting colloidal suspension upon the application of an electric field is commonly referred to as the electrorheological (ER) effect and such fluids have come to be known as ER fluids. These systems, which typically consist of small solid dielectric particles dispersed in an insulating host oil [1], undergo an increase in their shear viscosity, η, by several orders of magnitude, and exhibit a well-defined yield stress, τ_y, under shear flow conditions and sufficiently large electric field strengths($\sim$kV/mm) [1].

Since unelectrified ER dispersions are usually Newtonian fluids, the dramatic change in their rheological behavior can be explained in terms of a phase transition induced by the external field. The microstructure of the suspensions evolves from an initial liquid, disordered state to a final quasisolid configuration which should be distorted in order to make the suspension flow. However, this modification in the structure does not only affect the rheological properties but also the optical, acoustic, electrical, etc. characteristics of the ER systems giving rise to electro-optical, -acoustic, etc. effects [1,2].

Because of this possibility of obtaining a rapid, controllable modulation of the structure with an external excitation, interest has raised in ER fluids for practical applications, mainly in the field of electromechanics (hydraulics, robotics, and automotive industry). For instance, ER systems have been regarded as smart materials for active devices which transform electric energy into mechanical energy—such as actuators [3], torque transducers [4], and dampers [5]—or control the motion of liquids through a narrow channel in stop valves [6], clutches [7], and brakes [8]. Additionally, relating to the change in other physical (for example, optical) properties, we have also seen the development of new applications (alternative to mechanical devices) such as photonic crystals [9] or smart windows [10] based on the ER technology.

Although presently being used in some commercial devices, most of them are only prototypes. Their full potential has yet to be realized due to the absence of suitable materials for applications but mainly to the lack of a universal theory dealing with all the features of the ER effect.

The first record of the ER response of dielectric suspensions goes back to the experiments begun in 1939 (published in 1949 [11]) by W. M. Winslow, which is the reason why, this phenomenon is also referred to as Winslow effect. The next relevant research about ER fluids was carried out by Klass and Martinek and it is described in a series of papers outlining rheological an electrical properties [12,13]. Since that time, reports of research on ER fluids appeared sporadically until the 1980's, when the number of investigations increased dramatically because of the possibility of developing new ER materials (completely anhydrous powders, liquid crystals, complex etc. composites etc.) [1], more suitable for practical purposes. This impulse in tailoring ER fluids has

*Corresponding author. Present address: Departamento de Física Aplicada, Facultad de Ciencias, Avda. Fuentenueva s/n, 18071 Granada, Spain. FAX: +34-958243214. Electronic address: adelgado@ugr.es

TABLE I. Electrical properties (relative permittivity and conductivity) of hematite powder and silicone oil.

Material	Relative permittivity	Conductivity (S/m)
Iron oxide	10.9 ± 0.5	$(6.1 \pm 0.9) \times 10^{-2}$
Silicone oil	2.6 ± 0.1	$\sim 10^{-14}$

given rise to a renewed attempt to understand this phenomenon and a number of new theories (polarization [14], conduction [15], loss [16], microstructure models) have appeared since then.

However, despite the recent activity dealing with ER fluids and the improvement in the characterization of their properties, the ER effect is not completely understood yet. While most efforts have concentrated on the development of new formulations, surprisingly few investigations have taken into account the dynamic aspects of the ER effect. All theoretical models considered the interactions between particles in the structure of the suspensions once it is completely formed, but not the transition from the initial liquid to the final structured state. Similarly, the evolution of the induced structure under shear flow is usually studied in very dilute suspensions [17,18] but only a few researches (mostly computer simulations) have considered real (concentrated) ER fluids [19–22].

It is our intention in this paper to specifically focus on these dynamic characteristics of the ER effect under shear conditions. We begin with a description of the response of our selected ER fluid subjected to three shear tests: constant shear-rate, shear-rate sweeps, and hysteresis measurements, followed by a discussion of the relevant forces governing the properties of the suspensions. After that, we perform a structural analysis of the samples to finally elucidate its relationship with the observed rheological properties.

II. EXPERIMENTAL

A. Materials

Our selected ER fluid consisted of iron oxide (Aldrich, USA) dispersed in silicone oil (Fluka, USA) at a concentration of 11% in volume fraction. The solid phase consisted of irregularly shaped particles with a mean size, a_p, of 105 ± 25 nm and density $\rho_p = 5.24 \times 10^3$ kg/m^3. The nominal viscosity of the continuum medium, $\eta_m = 0.02$ Pa s, was chosen to be large enough to maximize the changes in the rheological properties induced by the electric field and, at the same time, minimize the effect of sedimentation of particles since the density of the silicone oil, $\rho_m = 9.68 \times 10^2$ kg/m^3, is significantly lower than ρ_p. The electrical properties (relative permittivity, ε, and conductivity, σ) of the solid (p) and liquid (m) phases were determined previously [23,24] and are summarized in Table I.

Samples were prepared as follows: the solid phase was slowly added to the silicone oil under vigorous shaking with a mechanical mixer (Atomixer, USA). No powder was added until the previously mixed material was well dispersed.

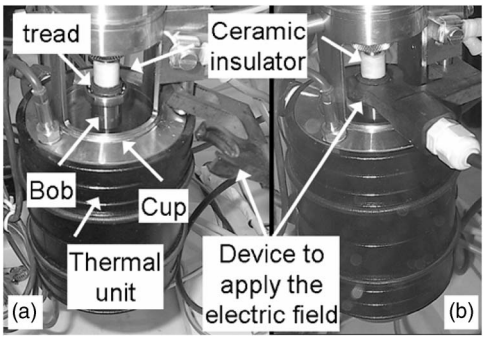

FIG. 1. (a) Photograph of the modified viscometer and the Couette cell to perform ER measurements. (b) Final configuration to allow the application of large electric fields.

Finally, the prepared ER fluid was stored in a desiccator to equilibrate the sample for 24 h before any measurement.

B. Experimental setup

The rheological measurements were carried out with a Haake VT550 viscometer (Germany), in a cylindrical Couette geometry SV1 ER. The diameters of the bob and cup were 20.2 and 22.2 mm, respectively, and the immersion length of the bob was 61.4 mm. We assume that the separation between concentric cylinders is narrow enough to neglect the variation of the shear rate inside the gap.

This equipment was modified so that high voltages could be applied to the samples. The internal cylinder, which rotates upon the application of a torque, was electrically insulated from the viscometer with a ceramic piece in order to prevent malfunctions induced by the large electric fields. This was supplied with a high voltage power generator and applied on a tread in the upper part of the bob while the cup was grounded (Fig. 1).

Experiments were performed at 25.0 ± 0.5 °C with the help of a Haake D8 thermostat (Germany) and a thermal unit covering the Couette cell (Fig. 1).

C. Methods

Three different types of rheological measurements were performed in order to determine the ER response of our samples:

1. Constant shear-rate tests

Samples were continuously sheared at $\dot{\gamma} = 0.0225$ s^{-1} for 150 s. After the first 30 s, a dc voltage was immediately applied, maintained for 90 s, and then suddenly removed while suspensions were kept under shear to complete the test. The magnitude of the electric field ranged from 1.5 to 3.5 kV/mm.

2. Shear rate sweeps

Each experiment was preceded by a period (90 s) of homogenization of the samples at high shear rate, $\dot{\gamma} = 200$s^{-1}, in absence of the electric field. In that way, the curves were well reproducible since we always started with a homogenous suspension and the same initial conditions.

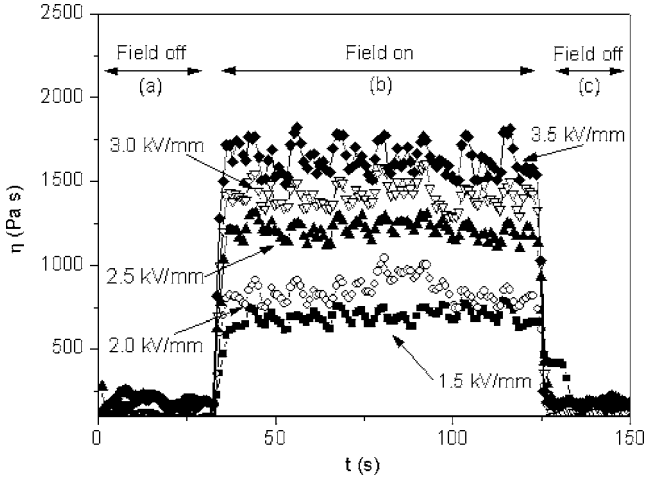

FIG. 2. Curves of shear viscosity vs time obtained from constant shear-rate tests. Samples are continuously sheared at $\dot{\gamma}=0.0225\ s^{-1}$ in absence—(a) and (c)—and presence—(b)—of different electric field strengths.

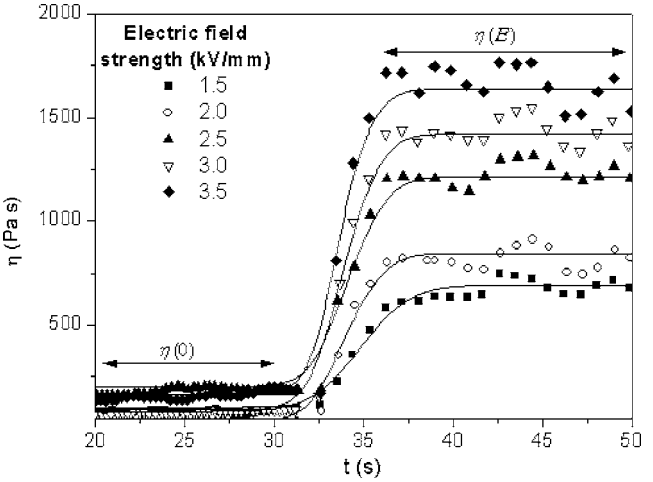

FIG. 3. Plots of the shear viscosity vs time at constant shear rate, as a function time in the presence of different field strengths. The field is applied at $t=30$ s. Lines correspond to the best fit to a Sigmoidal-Boltzmann curve [Eq. (1)].

After that, we applied an electric field (strength ranging from 1.5 to 3.5 kV/mm) to the quiescent sample for 15 s so that the above-mentioned phase transition, that is the formation of an induced structure, can take place.

Finally, our ER fluid was subjected to a steady state shear-rate sweep between 0.0225 and 200 s^{-1} for 90 s while the electric field was maintained.

3. Hysteresis measurements

This test was essentially the same as the sweeps that we have just described (including preshear and equilibration time conditions) although the shear rate, ranging between 0.0225 and 100 s^{-1}, was applied both in the increasing and decreasing directions (charge and discharge curves) for 180 s. The electric field strengths investigated were 1.5, 2.0 and 2.5 kV/mm.

Each dataset corresponding to a different electric field strength was measured at least three times to ensure the reproducibility of the results both in shear-rate sweeps and hysteresis measurements.

III. RESULTS

A. Constant shear-rate test

Figure 2 shows the change in the shear viscosity, η, with time, t, of our ER fluid when it is subjected to a constant shear rate and a squared-pulse electric field. Under the action of this external excitation, we can observe an abrupt increase in the viscosity, from a Newtonian, $\eta(0)$, to a field-induced value, $\eta(E)$, more pronounced the larger the magnitude of the applied field. This modification in the rheological behavior of the suspensions is completely reversible: shear viscosity dramatically decreases and reaches its initial Newtonian value once the electric field is switched off.

To elucidate how quickly this transient behavior in the hematite/silicone oil suspensions is, we have focused on the time range (Fig. 3) where the induced increase in the viscosity takes place (similar comments apply to the decrease interval). It can be observed that larger field strengths do not only provoke bigger values of the shear viscosity but also cause a reduction in the time required to reach those values.

We have quantified this evolution in the response of the suspension by just fitting the change in the shear viscosity to a typical growth function, the Sigmoidal-Boltzmann expression (Fig. 3)

$$\eta = \frac{\eta(0) - \eta(E)}{1 + \exp\left(\dfrac{(t - t_0)}{(t_{res}/4)}\right)} + \eta(E), \tag{1}$$

where t_0 is the time corresponding to a viscosity value $[\eta(0)+\eta(E)]/2$ and t_{res} is the response time required by the suspension to change from $\eta(0)$ to its final value $\eta(E)$. Results are shown in Fig. 4 where the viscosity increase, $\Delta\eta=\eta(E)-\eta(0)$, that is the net ER effect, and the response time, t_{res}, are plotted as functions of the electric field strength. $\Delta\eta$ linearly increases with the magnitude of the applied field, $\Delta\eta \propto E$, while t_{res} decreases according to an approximately hyperbolic power law, $t_{res} \propto E^{-1}$. These tendencies, the enhancement of the ER response and the decrease in the response time, have been obtained by other authors with different materials [25,26] although with field-squared dependence. An additional important point regarding the response time is that it is usually reported to be on the order of 10^{-3} s [17,25]. However, we have found that hematite/silicone oil suspensions need a few seconds to reach their maximum viscosity value. (For this reason, we have chosen 15 s as equilibration time in shear-rate sweeps and hysteresis measurements to be completely sure that the field-induced structure was formed.) We will comment on these differences later.

B. Shear-rate sweeps

Figure 5 shows the rheograms (a) and flow (b) curves obtained upon the application of different electric field

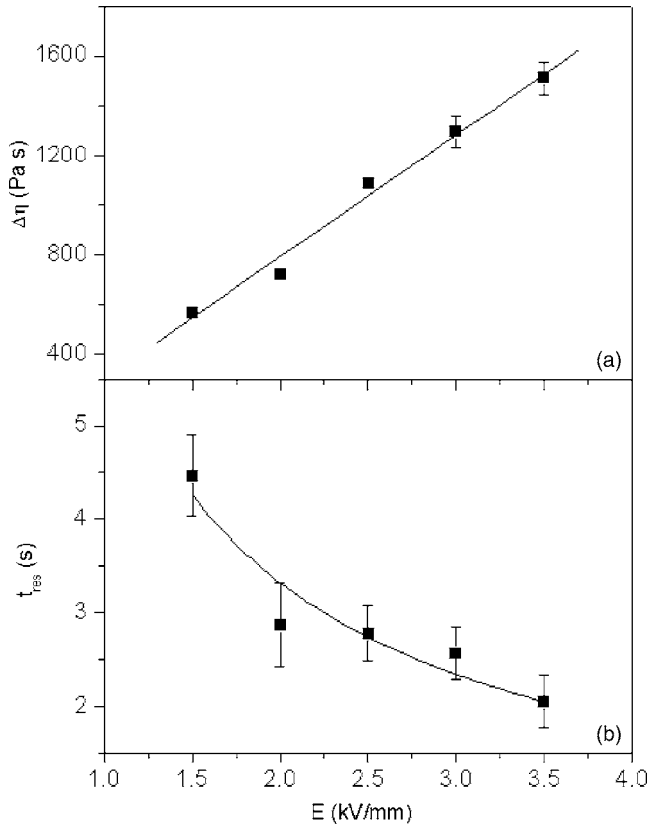

FIG. 4. Viscosity increase (a), $\Delta\eta=\eta(E)-\eta(0)$, and response time (b), t_{res}, vs electric field strength, E. Lines correspond to a linear (a) and an hyperbolic (b) functions, respectively: $\Delta\eta=a+bE$, $a=-190\pm90$, $b=492\pm33$, $\rho=0.99$. $t_{res}=cE^d$; $c=6.1\pm0.7$, $d=-0.87\pm0.16$, $\rho^2=0.91$. S. I. units.

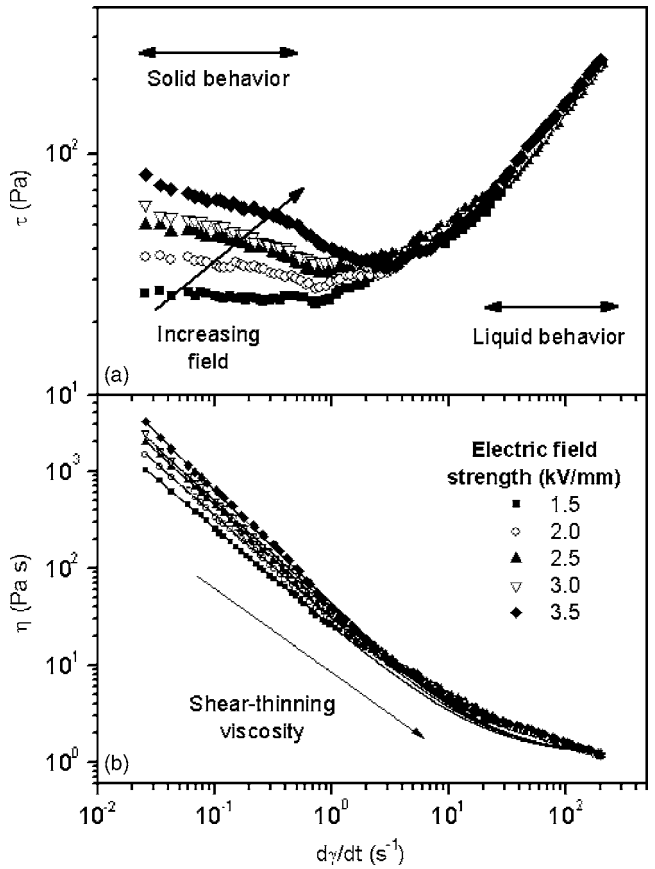

FIG. 5. Shear stress, τ (a), and shear viscosity, η(b), as functions of shear rate, $\dot{\gamma}$, for different electric field strengths, E. In part (b), lines correspond to a fit to the shear thinning model [Eq. (2)].

strengths. First of all, we must say that, in absence of electric fields, hematite/silicone oil suspensions behave as simple liquids with an approximately constant (Newtonian) viscosity $\eta(\infty)=1.157\pm0.001$ Pa s. However, a very different behavior is observed under the action of the external field. For instance, we can distinguish three different regions in shear stress, τ, curves [Fig. 5(a)]:

At very low shear rates ($\dot{\gamma}<0.5$ s^{-1}) τ remains approximately constant over this range of $\dot{\gamma}$. This constant value of the shear stress, the dynamic yield stress, τ_y, is typical of plastic systems and indicates that our ER fluids possess some kind of internal configuration: the structure induced by the external electric field. The applied shear field is only capable to slightly distort (but not destroy) the microstructure of particles within the electrified suspensions. Furthermore, we can also observe that larger E provokes higher τ_y in this region, reflecting a growing solidification of the systems and consequently a stronger structure in the dispersions.

On the other hand, for sufficiently large shear rates ($\dot{\gamma}>10$ s^{-1}), all curves merge, no matter the magnitude of the electric field, showing that this has little, if any, effect on the flow properties of the suspensions. Indeed, τ linearly depends on $\dot{\gamma}$, indicating that the samples exhibit the rheological properties as unelectrified ER fluids, that is, a simple Newtonian behavior. The strength of the shear field is large enough to completely overcome the action of the electric field to form any structure.

Finally, there is a third region, between the two previously described, at intermediate shear rates ($0.5<\dot{\gamma}<10$ s^{-1}) where the ER material exhibits a transition behavior: the shear stress (i.e., hydrodynamic interactions) continuously increases with $\dot{\gamma}$ until the field-induced structure of the suspension begins to be destroyed. In this range of shear rates, suspensions display viscoelastic properties, a mixed behavior between a solid and a liquid: there is some very weak structure in the ER fluid, although this is not strong enough to dominate the rheological properties.

Regarding the shear viscosity, η [Fig. 5(b)], the application of electric fields causes its increase, by three orders of magnitude with respect to the Newtonian value over the entire range of the evaluated shear rates. Similarly to the shear stress results, higher fields provoke larger increases in the shear viscosity at low shear rates while all curves approximately collapse for sufficiently pronounced shear fields: the electric field ceases to have any effect on the rheology of the suspension. Consequently the applied field provokes a shear-thinning flow in the dispersions: the shear viscosity enhancement is much larger at low shear rates and then substantially decreases until reaching the high shear rate viscosity, $\eta(\infty)$. Indeed, lines in Fig. 5(b) correspond to the fit of the shear viscosity to this shear-thinning model

$$\eta = a\dot{\gamma}^{-b} + \eta(\infty), \tag{2}$$

where a and b are the shear-thinning slope and exponent, respectively. Table II reflects the best fit parameters, and it

TABLE II. Best fit parameters of the shear viscosity [Fig. 5(b)] to the shear-thinning model [Eq. (2)], $\eta = a\dot{\gamma}^{-b} + \eta(\infty)$. ρ^2 is the determination coefficient.

Electric field strength (kV/mm)	Shear-thinning slope, a (S.I. units)	Shear-thinning exponent, b	High shear rate viscosity, $\eta(\infty)$ (Pa s)	ρ^2
1.5	24.1±0.3	−1.027±0.003	1.20±0.05	0.99955
2.0	29.5±0.3	−1.071±0.003	1.21±0.04	0.99964
2.5	34.7±0.4	−1.106±0.004	1.19±0.04	0.99949
3.0	38.3±0.4	−1.109±0.003	1.18±0.03	0.99966
3.5	42.0±0.7	−1.173±0.005	1.22±0.05	0.99931

can be observed that while b is approximately constant, a linearly increases with the field strength (Fig. 6). We will comment these particular tendencies in the next section.

C. Hysteresis measurements

Up to this point, we have evaluated the buildup of the structure in the ER suspension when it is subjected to an electric field, as well as the changes in the well-formed field-induced structure under the action of a progressively increasing shear field. We will now complete this study by considering the changes in the structure of the suspensions not only with shear rate but also with time, that is, hysteresis tests which only a very limited number of works about ER fluids have dealt with [27–29].

Figure 7 represents the rheograms (a) and flow curves (b) of the hysteresis tests obtained at different electric field strengths where the charge and discharge curves correspond to an enhancement and decreasing of the shear rate, respectively.

First, we must say that since the load and unload rheograms (and flow curves) obtained from unelectrified suspensions are indistinguishable, the differences observed in Fig. 7 are provoked by the application of the field. This causes a thixotropic behavior in the rheology of ER suspensions similarly to electrostatic interactions in clay dispersions, although, since the electric field is an external agent, we can easily control the thixotropy in ER fluids. Indeed larger electric fields provoke more pronounced yield stresses both in charge and discharge rheograms, although there is a net decrease in the difference between them, as Fig. 8 shows. We can observe that the loop area (area between the load and unload rheograms or flow curves), progressively reduces as the electric field strength is increased.

The determination of the loop area is a method to quantify this time evolution of the structures with shear and electric fields. When cycles of charge and discharge are performed in the presence of the external field, a memory effect is found

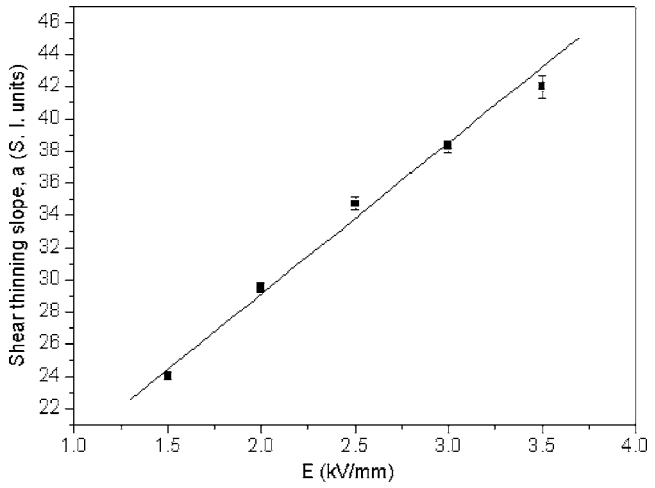

FIG. 6. Shear-thinning slope, a, vs electric field strength, E. Line corresponds to a linear fit.

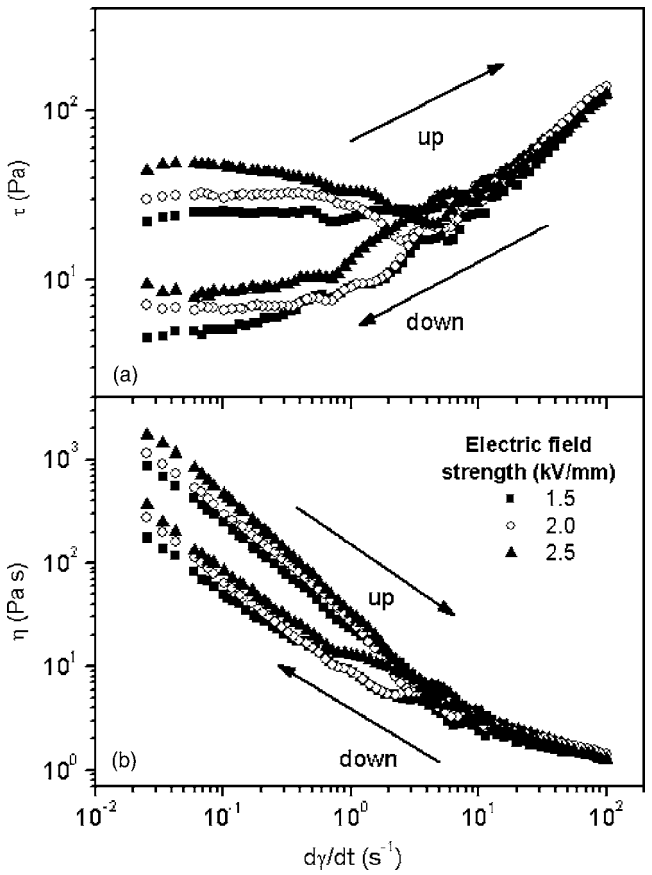

FIG. 7. Shear stress and shear viscosity of the hematite suspensions as a function of shear rate for the electric fields indicated. Experiments were performed both for increasing ("up") and decreasing ("down") shear rate.

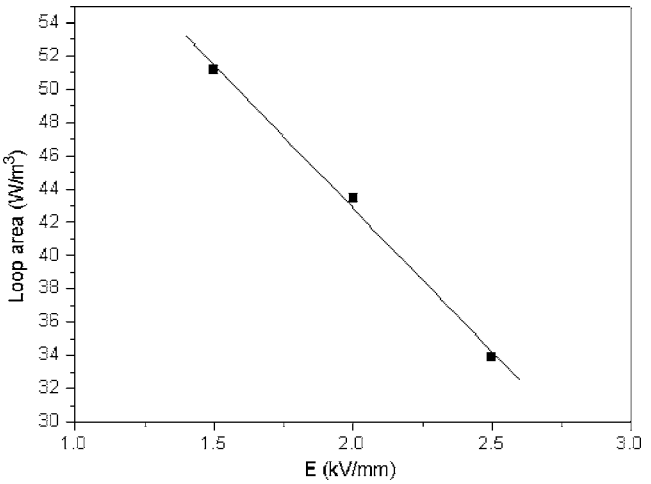

FIG. 8. Loop area (area between the "up" and "down" curves in Fig. 7) as a function of field strength.

which can be explained in terms of the macroscopic order inside the ER fluids: the final structure (unload curve) is significantly different from the one which is obtained when the field is switched on from a homogeneous suspension at rest (load curve). Two points should be commented about these results. On one hand, the structures in the discharge rheogram are not fully rebuilt as in the initial quiescent state, due to the disturbance of flow field: the action of the electric field is not enough to surpass the initial large shear rates (hydrodynamic forces). The induced structures cannot be reformed quickly enough so that, at a given applied field, the shear stress required to make the suspension flow is significantly smaller than in the load curve. On the other hand, there is a reduction in the loop area (i.e., thixotropy) of the rheograms (Fig. 8) when the magnitude of the external field increases because, at a fixed shear rate, the time required to form any structure on the suspension decreases with the applied field too [Fig. 4(b)].

IV. DISCUSSION

A. Identification of the interactions responsible for the ER effect in hematite/silicone oil suspensions

In order to completely understand the ER response exhibited by nonconducting colloidal systems, it is required to perform an analysis of both the interparticle interactions and the induced structures in the dispersion. These are the aims of the next sections. Let us consider first the fundamental forces acting on the particles in a suspension.

It is obvious that the ER effect can only be observed when the electric field is applied to the suspensions and provokes electrical interactions among dispersed solids. However, additionally to these, there are also other forces that (in the case of nonsterically stabilized systems such as our ER fluid) can be approximately described as follows [30]:

First of all, it should be taken into account the Brownian motion of particles which gives rise to a thermal interaction energy on the order of $\sim k_B T$, where k_B is the Boltzmann constant and T is the temperature.

TABLE III. Dimensionless ratios of the interaction energies between particles in an ER fluid. Calculated for $a_p=105$ nm, $\eta_m=0.02$ Pa s, $\varepsilon_m=2.6$, $T=298$ K, $\psi=5$ mV, $A=1k_BT$, $\delta_p=2.0$ nm and $\dot{\gamma}$ between 0.025 and 200 s^{-1}.

Interactions	Characteristic dimensionless number	Ratio
Viscous / Thermal	$\frac{6\pi\eta_m a_p^3\dot{\gamma}}{k_BT}$	0.027–21.22
Electrostatic / Thermal	$\frac{4\pi\varepsilon_0\varepsilon_m a_p\psi^2}{k_BT}$	0.18
van der Waals / Thermal	$\frac{Aa_p}{24\delta_p k_BT}$	2.08

The ubiquitous London-van der Waals forces between any two bodies provoke an additional interaction energy $Aa_p/(24\delta_p k_B T)$. Here, A is the Hamaker constant and δ_p the surface roughness of the particles which typically verifies $\delta_p/a_p=10^{-2}-10^{-3}$.

Associated to any particle dispersed in a liquid medium, there is an ionic double layer and therefore an electrostatic interaction energy between close particles $4\pi\varepsilon_0\varepsilon_m a_p\psi^2$, where ψ is the electrostatic surface potential.

Finally, since ER fluids are also subjected to shear forces it is necessary to consider the viscous or hydrodynamic interaction energy, $6\pi\eta_m a_p^3\dot{\gamma}$.

Table III shows the typical ratios between these energies for hematite/silicone oil suspensions in our current experimental conditions. We can observe that double-layer forces are not important in ER fluids since their electrostatic surface potential is negligible in nonconducting suspensions [31]: ER fluids have very small surface charge densities in comparison with aqueous systems. On the other hand, thermal and London-van der Waals are more important than viscous forces at low shear rates, where a more pronounced ER effect is observed (Figs. 5 and 7). Consequently, under these experimental conditions, the field-induced electrical forces dominate the system and are not affected by the magnitude of these interactions. Only at high shear rate the importance of the electrical forces decreases because of the large magnitude of the hydrodynamic interactions, which are significantly larger than the London-van der Waals and Brownian contributions. As a first conclusion of this analysis we can say that, even for small field strengths, the electrical forces (F_{elec}) entirely determine the induced structure in suspensions, which may be only affected by large hydrodynamic forces (F_{hydro}). The next step of our research will precisely deal with obtaining more information about them.

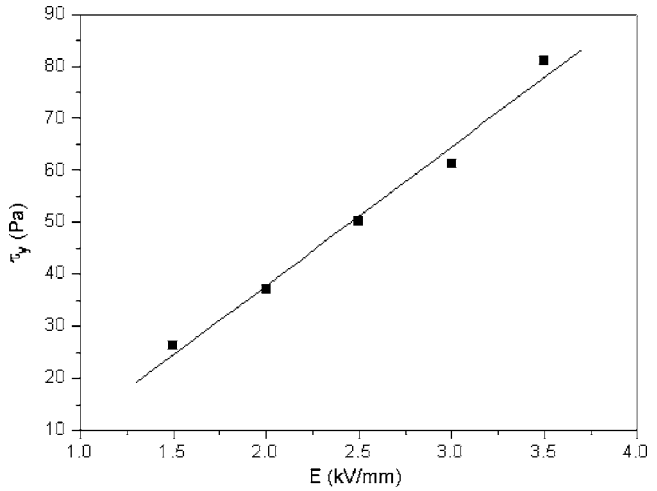

FIG. 9. Dynamic yield stress, τ_y, as a function of the electric field strength, E. Line corresponds to a linear fit: $\tau_y = r + sE$; $r = -15.6 \pm 4.7$ Pa; $s = 26.7 \pm 1.8$ [Pa (kV/mm)$^{-1}$]; $\rho = 0.99$.

B. ER effect and electrical forces

Since unelectrified suspensions are Newtonian, the appearance of a well-defined yield stress [Fig. 5(a)] should reflect the action of the applied electric field on the samples ($\tau_y \propto F_{elec}$). We have plotted τ_y (taking τ at 0.0225 s^{-1} as reference value) as a function of the electric field strength, E (in absolute value: the ER effect will depend on some power of the field strength, but not on its direction) in Fig. 9. A linear relationship can be observed between these two quantities, and several consequences can be extracted from this result:

(i) The electrical forces acting on the particles in the suspensions are proportional to the field strength (not the field squared as it is usually reported [14]). This explains why the viscosity increase, $\Delta\eta$, in Fig. 4(a), which reflects the net change in the shear viscosity provoked by the external field, linearly increases with E.

(ii) Stronger electrical interactions give rise to shorter response times. Since electrical forces linearly depend on the field strength, it follows that $t_{res} \propto E^{-1}$ rather than the typically found $t_{res} \propto E^{-2}$ [25,26].

(iii) The linear relationship, $\tau_y = r + sE$, between the yield stress and the field strength provides additional information about the ER effect. It suggests the existence of a critical electric field, $E_c = -r/s$ (note that E_c is positive, as it should, since the the intercept r is negative), below which it is not possible to observe any ER response (a net yield stress). It has been experimentally found, from structural observations [18], that a fully-developed structure extending from one electrode to the other does not occur until a critical field is exceeded, whose measured value resulted to be on the order of $E_c = 0.5$ kV/mm, agreeing with that obtained from the best fit parameters of Fig. 9, $E_c = 0.58 \pm 0.22$ kV/mm.

On the other hand, the origin of the ER effect has been commonly ascribed to the alignment of the particles of a suspension into chainlike fibrils. Particles get polarized—because of the action of the external field but also because of the field associated to the rest of polarized solids—and attract each other according to anisotropic electrical forces causing their aggregation. The time required for the formation of the first pseudochains (composed by only a few particles) is on the order of 1–10 ms, which should not be identified with the response time of the ER suspension, that in fact corresponds to the final development of a complete structure spanning the large gap between the electrodes. This process may take substantially longer, even on a time scale of seconds in certain cases [33,34] as it happens for hematite/silicone oil suspensions.

According to the simplest description, the Maxwell-Wagner model, the polarization of the particles is due to the mismatch in the electric properties between the solid and liquid phases. At high ac electric fields, the difference in permittivities dominate the polarization of the solids, however for dc and low ac electric fields, this process is completely determined by the conductivity mismatch [14]: the conductivity of the ER suspension results in the accumulation of charge at the particle/fluid interface screening the field within a particle. For high ac fields the mobile charges have not enough time to follow the applied field so that the polarization is solely dominated by permittivities. This explanation justifies the usually found dependence between the yield stress (i.e., the electrical forces) and ac electric fields, $\tau_y \propto F_{elec} \propto E^2$ [14,23].

This picture is nonetheless so simple for dc or low ac excitations. The E^2 dependence is only found for low magnitude of the applied field but it is frequently less than quadratic for large dc electric field strength and high ratios of conductivities of the solids and liquid phases [14,15,26,35]. That is the case of hematite/silicone oil suspensions ($\sigma_p \geqslant 10^{-7}$ S/m and $\sigma_m \geqslant 10^{-14}$ S/m) as the results in Fig. 9 reflects, and this cannot be simply explained by the polarization model, so that additional processes should be taken into account.

Indeed, the justification of this deviation is related to the modification of the conductivity of the host oil, σ_m, with the magnitude of the field. For sufficiently large external dc electric fields, the local field among close particles (and between particles and the electrodes) produce the dissociation of impurities dispersed in the liquid medium [15] as well as charge injection from the electrodes to the bulk of the suspension [35]. These processes in turn give rise to a field enhancement in the conductivity of the silicone oil and a saturation of the electrical forces among particles, $F_{elec} \propto E^n$ with $n < 2$ [36], more pronounced the higher the conductivity of the solid phase. A complete study of this phenomenon, that is, the role of the field strength on the conductivity of the samples (more properly, the silicone oil) and the subsequent effect on their induced structure, can be found in [24] where several electric field strengths were applied to quiescent hematite/silicone oil suspensions in a very diluted regime (in order to distinguish more easily different groups of particles). We observed that at low electric fields, chainlike structures were formed, indicating the preponderance of pure polarization forces. However, when the magnitude of the applied field increases ($E \geqslant 0.5$ kV/mm), a chaotic motion of aggregates of particles between the electrodes appears. This migration of clusters indicated that particles acquire a net charge which can be solely produced by the field-induced dissociation of the silicone oil between closing particles and charge injection from

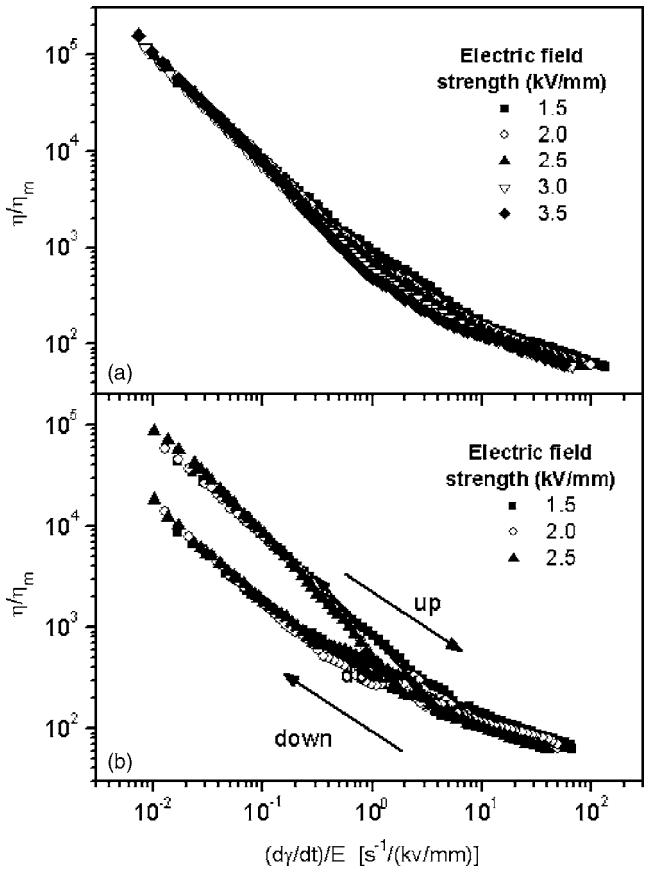

FIG. 10. Relative viscosity (viscosity of the suspension, η, divided by that of the medium, η_m) as a function of the ratio between the shear rate, $\dot{\gamma}$, and the field strength, E. (a): data from shear-rate sweeps (Fig. 5); (b): data from hysteresis tests (Fig. 7).

the electrodes to the bulk of the suspensions.

Summarizing, the previous analysis leads to a simplification in the study of the ER response since particles may be approximately considered as hard solids interacting through viscous ($F_{hydro} \propto \dot{\gamma}$) and electrical ($F_{elec} \propto E$) forces alone. In fact, when we plot (Fig. 10) the relative viscosity, η/η_m, vs the ratio $F_{hydro}/F_{elec} \propto \dot{\gamma}/E$, it can be observed that the ER effect is completely explained in terms of a balance between these two forces through the expression

$$\frac{\eta}{\eta_m} = k\left(\frac{\dot{\gamma}}{E}\right)^{-1} + \frac{\eta(\infty)}{\eta_m}, \tag{3}$$

where k depends on the electrical properties of the solid and liquid phases, and the concentration of particles, and it also includes a structural factor related to the field-induced internal arrangement in the suspension [23,32]. All experimental data collapse on this single master curve independently of the electric field strength and the type of rheological test, either shear rate sweeps [Fig. 10(a)] or hysteresis measurements [Fig. 10(b)]: the only difference between the load and unload flow curves is that in the latter case the structural factor included in k is significantly lower due to weaker structures, as we have explained above.

Finally, since the constitutive equation of any ER fluid [Eq. (3)] displays a shear-thinning behavior, it can now be explained the particular behaviors of the shear-thinning slope, a and exponent, b in Table II and Fig. 6: they reflect that the electrical and hydrodynamic interactions are the only forces governing the observed ER response, as well as the linear dependence of the former with the field strength.

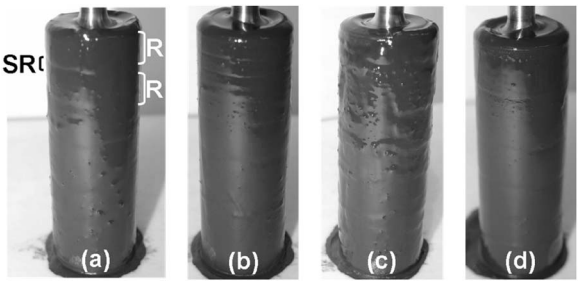

FIG. 11. Photos of the rings (R) of particles, and of the slip regions (SR) between them, formed on the surface of the bob at different experimental conditions: (a) $E=2.5$ kV/mm, $\dot{\gamma}=0.03$ s^{-1}; (b) $E=2.5$ kV/mm, $\dot{\gamma}=1$ s^{-1}; (c) $E=2.5$ kV/mm, $\dot{\gamma}=20$ s^{-1}, and (d) $E=3.5$ kV/mm, $\dot{\gamma}=0.03$ s^{-1}. The ratio of the gap between adjacent rings, SR, and the average size of a lamella, R, is SR/R=0.29 and 0.09 for the experimental conditions (a) and (d), respectively.

C. ER effect and field-induced structures

Another important point to be taken into account is the type of structural arrangement in ER suspensions. There are numerous publications showing the formation of chains as well as the breaking of these fibrils under the action of a shear field. However, all these observations were obtained on microscope slides at very dilute concentrations of particles. In this situation, the observed chains effectively consist of individual fibrils whose thickness is on the order of one particle diameter [37]. However, this is not always true. Indeed, slightly more concentrated (but still dilute) samples give rise to imperfections in the chainlike structure: chain cross links and debris of fibril segments are produced, as well as an increase in the thickness of the chains [18]. All these findings suggest that the real structure in concentrated ER fluids really consists of aggregates of clusters of particles instead of individual chains. The small gap between electrodes, the reduced particle size, and, mainly, the opacity of the samples make it very difficult to get direct observations of these structures, particularly in real flow conditions. All these problems have discouraged significant research effort in this area and, for this reason, the ER effect is often identified with the simple mechanism of chain breaking even for concentrated samples.

We have tried to contribute to this issue of the effect of the shear field on the structure of the samples. To overcome the above mentioned difficulties, we have considered the appearance of the bob and cup once rheological tests (in the investigated samples, without dilution) have finished. This alternative procedure is not worry free either, since the possible structures on the surface of the concentric cylinders can be easily destroyed when they are removed from the rheometer. Nevertheless, if this operation is carefully carried out some information can be extracted. Fig. 11 shows some of the structural patterns formed on the bob under different ex-

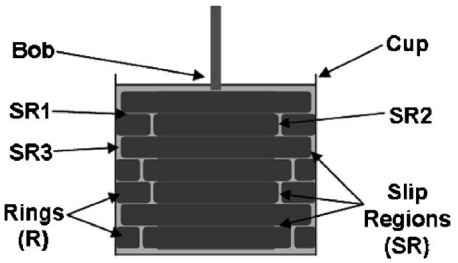

FIG. 12. Scheme of the pattern of rings formed in an ER fluid simultaneously subjected to an electric and a shear field. R: rings, SR: slip region which may appear between adjacent lamellas (SR1), inside a ring (SR2), and between the free end of a lamella and the opposite electrode (SR3).

perimental conditions (similar pictures can be observed on the cup).

First of all, we can see that particles appear to accumulate on some regions of the cylinder [Fig. 11(a)]. These groups of aggregates have cylindrical symmetry so that they can be described as rings (R) or lamellas of solids in between which we can find regions almost free of particles (SR). Only under the simultaneous application of shear and electric fields can these rings develop: if either the electric or the shear field is not present, a homogenous distribution of particles along the measurement cell is observed. It is also worth mentioning that the formation of this structural pattern is not a specific property of our ER fluid or an artifice of the used viscometer. Similar rings have been observed with ER fluids of different compositions, several rheological testers, and numerous measurement cells [21,22].

Regarding the structural properties of these lamellas, we have found that their thickness and the distance between them are complex functions of many factors. We have investigated two of them: the shear rate and the electric field strength.

Under the same magnitude of the applied field, $E=2.5$ kV/mm, an enhancement of the shear rate, from 0.3 [Fig. 11(a)] to 1.0 s^{-1} [Fig. 11(b)], provokes an increase in the number of rings, which are also better defined. A further increase in the shear rate [Fig. 11(c), $\dot{\gamma}=20$ s^{-1}], by contrast, gives rise to a partial destruction of the lamellas.

The electric field also has a remarkable effect on the formation of these lamellas. When the magnitude of the applied field increases, samples subjected to the same shear field ($\dot{\gamma}=0.3$ s^{-1}) exhibit thicker and more defined rings and a reduction in the region free of particles between them [Fig. 11(d)].

These new structural patterns provide an alternative qualitative explanation to the observed ER response, particularly for concentrated samples. The resistance to flow is not due to chain breaking but to the shearing of the liquid medium (the silicone oil) in the possible slip regions (SR), the regions free of particles (Fig. 12). Slip may occur in between a single ring when it is adhered to both electrodes (SR1), or in the lateral surfaces of adjacent rings (SR2) and/or the free end of a lamella with the opposite electrode (SR3), when it is adhered to only one electrode.

On the other hand, it is interesting noting that, independently of the formed structural pattern, the observed ER effect is, of course, the result of a competition between the electrical and viscous interactions and the subsequent changes provoked on the structure of the suspensions (Fig. 13) as we have demonstrated in the previous section. The electrical forces tend to keep the integrity of the rings by maintaining their particles together, while the hydrodynamic forces give rise to the passage of the silicone oil between the rings causing their progressive deterioration. At very low shear rates, the initial quiescent structure of aggregates of particles starts to be distorted and rings quickly begin to be formed [Fig. 11(a)] until a further moderate increase in $\dot{\gamma}$ gives rise to the final development of all the possible lamellas [Fig. 11(b)]. Up to these shear rate values, samples still exhibit a yield process (characterized by a constant shear stress in the rheograms and large values of η in the flow curves) since a complete structure (the pattern of rings) still can be observed between the electrodes. Electrical forces are predominant on the suspensions as the lamellas keep their integrity and the shear field only provokes a slight deformation (or better said, a reordering) of the initial induced structure. However, the application of increasingly high shear rates progressively destroys the rings of particles [Fig. 11(c)], and the resistance to flow continuously decreases until samples reach a liquidlike behavior. Under these conditions, the hydrodynamic forces completely dominate over the electrical interactions: the electric field ceases to have a net effect on the rheology of the suspension.

Higher field strengths give rise to stronger interactions between particles and consequently to rings which are more resistant to shear forces. However, the enhancement of the ER effect provoked by the applied field is not only limited to the strength of the interactions but also to the structural changes in the suspensions. For low field strengths [Fig. 11(b)], shear gradients between consecutive rings may be small, because of the large size of SR1. Consequently, the observed enhancement in the viscosity of the samples should be mainly due to the slip of the silicone oil between the ends of the lamellas and the electrodes (SR2) and inside a ring simultaneously adhered to the bob and cup (SR3). Larger magnitudes of the applied field originate thicker rings [Fig. 11(d)], increasing the shearing areas SR2 and SR3, while reducing the SR1 gaps. All these changes cause additional energy dissipations and a subsequent stronger ER effect.

A number of models have been suggested to explain the formation of chains or aggregates of particles between the electrodes, but actually the way in which the passage from this structure to a phase of dense domains of rings takes place remains unclear in the ER effect.

The formation of the lamellas in magnetorheological (MR) fluids (the analogue of ER fluids for magnetic fields) has been successfully explained by a model [38] based on the minimization of the magnetic energy and on the equilibrium of osmotic, hydrodynamic, and magnetic pressures. However, this model is not applicable to ER materials, since the presence of a well defined pattern of rings in magnetic fluids is due to depolarization effects which do not exist in ER fluids. This difference is related to the fact that the boundary conditions are different: in ER fluids, it is not the external field that is fixed but the internal field (the Maxwell field), and there is no equivalent of the demagnetization fac-

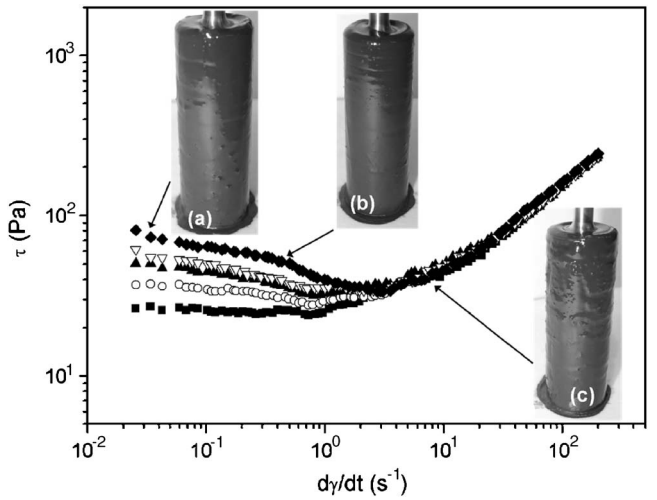

FIG. 13. Shear stress curves [same as Fig. 5(a)] and the associated structures of the suspension [Figs. 11(a)–11(c)] for different shear rates.

tor since the charges on the electrodes will adjust in order to keep the internal field constant.

Other models, mainly numerical simulations, have been proposed by different authors to explain the lamellar structures in ER fluids [19,39]. The most successful attempt has been performed by Von Pfeil *et al.* [20]. They developed a mass transport model where the particle flux is related to the divergence of the particle contribution to the stress, which in turn is related to the suspension dielectric and electrostrictive properties. Solutions of the resulting particle conservation equation capture the column formation in quiescent suspensions and the stripe formation in sheared samples. Additionally, the model reproduces the experimental findings about the increase in thickness and number of lamellas with shear rate.

Despite the apparent success of these simulations to justify the existence of the rings, they present some important limitations in the description of ER materials and their actual ER response. These models only take into account monodisperse spherical particles and pure dipolar forces, $F_{elec} \propto E^2$, due to the dielectric mismatch between the solid and liquid phase. However, as we have shown in Fig. 9, conductivity (electrochemical) effects are important in ER fluids, especially for dc fields, causing the saturation of electrical forces which actually depend linearly on the field strength. Furthermore, electric currents play an important role in ER effect [15,26,35]. These points are not considered in these simulations, which in fact, assume both ER fluids and electrical forces as simply equivalent to MR suspensions and magnetic interactions by just changing electric by magnetic permittivities. All these aspects, as well as the lack of suitable tests allowing a better description of the transition from aggregates to rings in real time make it necessary to perform further research about the theoretical and experimental characterization of the dynamic evolution of the structure of ER materials.

V. CONCLUSIONS

The present work contains a complete description of the hematite/silicone oil suspensions as a model of ER fluid. Analyses of their rheology as well as of the interactions between the particles, together with investigations of the structure of the electrified fluids, have been performed to understand the ER effect displayed by these suspensions.

Constant shear rate tests show that the actual ER response of these materials takes substantially a longer time than typically reported ($\sim 10^{-3}$ s), and actually the observation of the maximum viscosity increase can take several seconds. Conventional shear-rate sweeps show a well defined shear-thinning plastic behavior where an evolution from solid to liquid behavior can be observed via a viscoelastic transition. On the other hand, hysteresis measurements reflect that ER fluids posses a memory effect associated with a thixotropic behavior which is less significant the higher the field strength.

The study of the fundamental forces involved in an electrified colloidal suspension was the first step to clarify the observed ER response. Thermal, double-layer, and London-van der Waals interactions resulted to be negligible in comparison with hydrodynamic and electrical forces in ER fluids. The latter were investigated by means of the yield stress exhibited by the samples. This quantity does not only reflect that electrical forces linearly depend on the electric field, but also shows the existence of a critical field strength (below which no ER effect appears) and explains the particular decrease of the response time with the applied field.

Finally, we have also studied the evolution of the field-induced structure in suspensions simultaneously subjected to shear and electric fields. Appearance of a well-defined pattern of rings takes place provided that the shear rate is not excessively large. In this case, destruction of the mentioned rings occurs, and a liquid behavior is observed in the flow curves. By contrast, at low shear rates, the pronounced increase in the viscosity (the ER effect) is due to the shearing of the liquid phase inside rings and/or between them and the electrode surfaces. This structural analysis reflects that the action of the electric field is not only related to the increase in the electrical forces but also to the modification of the formed rings giving rise to closer and larges shearing surfaces.

ACKNOWLEDGMENTS

Financial support from the Spanish Ministry of Science and Technology and Feder Funds (EU) (Project FIS2005-06860-CO2-1) is acknowledged. One of us (M.J.E.) wishes to thank the Spanish Ministry of Education for the Grant covering this research work.

[1] T. Hao, Adv. Colloid Interface Sci. **97**, 1 (2002).
[2] J. M. Ginder, Phys. Rev. E **47**, 3418 (1993).
[3] S. B. Choi, Y. K. Park, and M. S. Suh, AIAA J. **32**, 438 (1993).
[4] D. L. Hartsock, R. F. Novak, and G. J. Chuandy, J. Rheol. **35**, 1305 (1991).
[5] R. Stanway, J. L. Sproston, and A. K. El-Wahed, Smart Mater. Struct. **5**, 464 (1996).
[6] Y. F. Deniega and G. V. Vinogradov, Rheol. Acta **23**, 636 (1984).
[7] W. A. Bullough, A. R. Johnson, R. Tozer, and J. Makin, in *Proceedings of the International Conference on Electrorheological Fluids*, Yonezawa, 1997, edited by M. Nakano and K. Koyuama (World Scientific, Singapore, 1998), p. 201.
[8] J. Furusho, M. Sakaguchi, N. Takesue, and K. Koyanagi, J. Intell. Mater. Syst. Struct. **13**, 425 (2002).
[9] R. Tao, Appl. Phys. Lett. **80**, 4702 (2002).
[10] H. Tada, Y. Saito, M. Hirata, M. Hyodo, and H. Kawahar, J. Appl. Phys. **73**, 489 (1993).
[11] W. M. Winslow, J. Appl. Phys. **20**, 1137 (1949).
[12] D. L. Klass and T. W. Martinek, J. Appl. Phys. **38**, 67 (1967).
[13] D. L. Klass and T. W. Martinek, J. Appl. Phys. **38**, 75 (1967).
[14] M. Parthasarathy and D. J. Klingenber, Mater. Sci. Eng., R. **17**, 57 (1996).
[15] C. Boissy, P. Atten, and J. N. Foulc, Int. J. Mod. Phys. B **10**, 2991 (1996).
[16] T. Hao, A. Kawai, and F. Ikazaki, Langmuir **16**, 3058 (2000).
[17] D. J. Klingenberg and C. F. Zukoski, Langmuir **6**, 15 (1990).
[18] H. Conrad, Y. Chen, and A. F. Sprecher, Int. J. Mod. Phys. B **6**, 2575 (1992).
[19] J. R. Melrose and D. M. Heyes, J. Chem. Phys. **98**, 5873 (1993).
[20] K. Von Pfeil, D. Grham, D. J. Klingenberg, and J. F. Morry, J. Appl. Phys. **93**, 5769 (2003).
[21] S. Henley and F. E. Filisko, J. Rheol. **43**, 1323 (1999).
[22] S. L. Vieira, L. B. Pompeo Neto, and A. C. F. Arruda, J. Rheol. **44**, 1139 (2000).
[23] M. J. Espin, A. V. Delgado, and J. E. Martin, Rheol. Acta **44**, 71 (2004).
[24] M. J. Espin, A. V. Delgado, and S. Ahualli, IEEE Trans. Dielect. Electr. Insulation (to be published).
[25] T. C. Halsey, Science **258**, 761 (1992).
[26] P. Atten, J. N. Foulc, and N. Felici, Int. J. Mod. Phys. B **8**, 2731 (1994).
[27] H. J. Choi, M. S. Cho, and M. S. Jhon, Int. J. Mod. Phys. B **13**, 1901 (1999).
[28] H. Block, J. P. Kelly, A. Quin, and T. Waston, Langmuir **6**, 6 (1990).
[29] Y. Z. Xu and R. F. Liang, J. Rheol. **35**, 1355 (1991).
[30] A. P. Gast and C. F. Zukoski, Adv. Colloid Interface Sci. **30**, 153 (1989).
[31] D. Brooks, J. Goodwin, C. Hjelm, L. Marshall, and C. Zukoski, Colloids Surf. **18**, 293 (1986).
[32] J. E. Martin and R. A. Anderson, J. Chem. Phys. **104**, 4814 (1996).
[33] Y. Otsubo and K. Edamura, J. Non-Newtonian Fluid Mech. **71**, 183 (1997).
[34] A. F. Sprecher, J. D. Carlson, and H. Conrad, Mater. Sci. Eng. **95**, 187 (1987).
[35] N. J. Felici, J. Electrost. **40-41**, 567 (1997).
[36] M. J. Espin, A. V. Delgado, and J. Płocharski, Rheol. Acta
[37] D. J. Klingenberg, MRS Bull. **23**, 30 (1998).
[38] S. Cutillas, G. Bossis, and A. Cebers, Phys. Rev. E **57**, 804 (1998).
[39] J. E. Martin, Phys. Rev. E **63**, 011406 (2000).